Supplementary Information (SI) for New Journal of Chemistry.
This journal is © The Royal Society of Chemistry and the Centre National de la Recherche Scientifique 2024

Supporting Information

Positional Effects of Fluorine Substitution on Room Temperature Phosphorescence in Hexaphenylmelamine Derivatives

Qiang Guo[a,d], Zixuan Huang[a], Jiaqi Liu[a], Xiaoyu Li[b], Yanqiong Zheng[c], Xiuying Gao*[a,e], Hui Liu*[a], Jie Li*[a]

[a] *College of Optoelectronic Engineering, Chengdu University of Information Technology, Chengdu 610225, China.*

[b] *Southwest University of Science and Technology, Mianyang 621010, China*

[c] *Key Laboratory of Advanced Display and System Applications of Ministry of Education, School of Mechatronic Engineering and Automation, Shanghai University, Shanghai 200072, China.*

[d] *HONGCHANG Chem. Co., Ltd. Guangdong*

[e] *TRULY (Renshou) High-End Display Technology Limited*

** E-mail: lijie@cuit.edu.cn*

Table of Contents

I. General remarks

1. Materials

Unless otherwise noted, diphenylamine, cyanuric chloride, *n*-BuLi (2.5 M in hexane) and extra dry solvents (THF stored with molecular sieves) were obtained from commercial suppliers and used without further purification. 2-Fluoro-*N*-phenylaniline, 3-fluoro-*N*-phenylaniline [S1], 4-fluoro-*N*-phenylaniline [S2] and 2-chloro-4,6-bis(diphenylamino)-1,3,5-trazine [S3] were prepared according to the literatures.

2. Instrumentation

NMR spectra were obtained on a Varian Inova 400 spectrometer. The ^{1}H NMR (400 MHz) and ^{13}C NMR (100 MHz) chemical shifts were measured relative to $CDCl_3$ as the internal reference ($CDCl_3$: δ = 7.26 ppm for ^{1}H and δ = 77.16 ppm for ^{13}C, respectively). High-resolution mass spectra (HRMS) were obtained with Waters-Q-TOF-Premier (ESI^{+}). Single-crystal X-ray diffraction data for the compounds were obtained by using Bruker APEX-II CCD diffractometer with Mo radiation (for HPM-*o*-F and HPM-*m*-F) or a New Gemini, Dual, Cu at zero, EosS2 diffractometer (for HPM-*p*-F) at 298.00 K during data collection. Using Olex2 [S4], the structure was solved with the ShelXT [S5] structure solution program using Intrinsic Phasing and refined with the ShelXL [S6] refinement package using Least Squares minimisation (for HPM-*o*-F and HPM-*m*-F) or with olex2.refine [S7] refinement package using Levenberg-Marquardt minimisation (for HPM-*p*-F). Photoluminescence measurements at 77K were carried out by FLS-920 spectrophotometer. Room-temperature phosphorescence (RTP) spectra were measured using HITACHI F-7100 FL spectrophotometer (phosphorescence mode, chopping speed: 40 Hz). The RTP lifetimes were collected on a HORIBA TEMPRO-01 instrument. The phosphorescence quantum yields were determined by FLS-980 with integrating sphere systems under ambient conditions.

II. Synthesis procedures

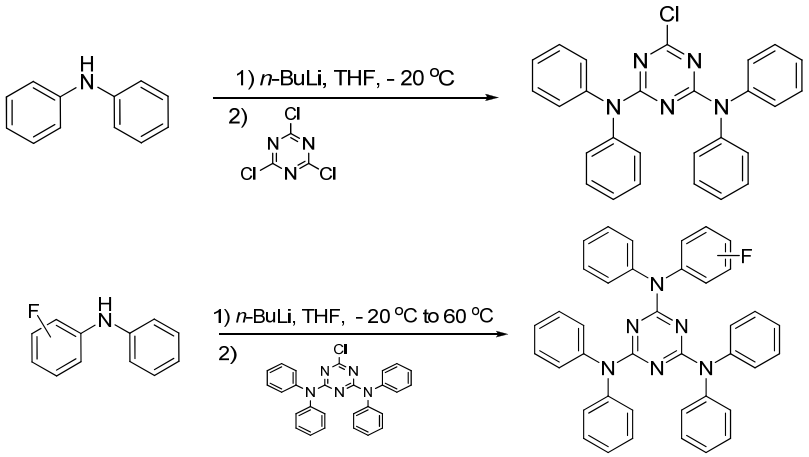

Scheme S1 Synthesis of HPM-F isomers.

2-[*N,N*-(2-fluorophenyl)phenylamino)]-4,6-bis(diphenylamino)-1,3,5-trazine (HPM-*o*-F): 4-Fluoro-*N*-phenylaniline (617.8 mg, 3.3 mmol) and 30 mL dry THF were palced in a flame-dried Schlenk tube with a magnetic stir bar under a N_2 atmosphere. Then the solution was cooled to -20 °C and *n*-BuLi (2.5 M in hexane, 1.45 mL, 3.63 mmol) was dropped slowly into the solution. The mixture was then warmed to room temperature and 2-chloro-4,6-bis(diphenylamino)-1,3,5-trazine (1.35 g, 3 mmol) was added. The mixture was heated at 60 °C overnight. A large amount of solid product was precipitated. The precipitation was filtered and washed with ethanol several times. The desired product was then recrystallized from xylene and dried in vacuo to give a white solid (760 mg, 42%). ^{1}H NMR (400 MHz, $CDCl_3$): δ = 7.08-7.17 (m, 22 H), 7.00-7.05 (m, 5H), 6.93-6.97 (m, 2H) ppm. ^{13}C NMR (100 MHz, $CDCl_3$): δ = 165.9, 165.6, 160.0, 157.5, 143.6, 142.6, 130.3, 128.3, 128.2, 127.9, 127.8, 127.6, 126.5, 125.0, 124.9, 124.3, 116.4, 116.2 ppm. HRMS (ESI^+): calcd. for $C_{39}H_{29}FN_6$, $[M+H]^+$ 601.2516, found 601.2519.

2-[*N,N*-(3-fluorophenyl)phenylamino)]-4,6-bis(diphenylamino)-1,3,5-trazine (HPM-*m*-F): 4-Fluoro-*N*-phenylaniline (280.8 mg, 1.5 mmol) and 10 mL dry THF were palced in a flame-dried Schlenk tube with a magnetic stir bar under a N_2 atmosphere. Then the solution was cooled to -20 °C and *n*-BuLi (2.5 M in hexane, 0.72 mL, 1.8 mmol) was dropped slowly into the solution. The mixture was then warmed to room temperature and 2-chloro-4,6-bis(diphenylamino)-1,3,5-trazine (449.9 mg, 1 mmol) was added. The mixture was heated at 60 °C overnight. A large amount of solid product was precipitated. The precipitation was filtered and washed with methanol several times. The desired product was then recrystallized from xylene and dried in vacuo to give a white solid (334 mg, 56%). ^{1}H NMR (400 MHz, $CDCl_3$): δ = 7.00-7.17 (m, 26 H), 6.82-6.92 (m, 2H), 6.69-6.73 (m, 1H) ppm. ^{13}C NMR (100 MHz, $CDCl_3$): δ = 165.8, 165.7, 143.5, 143.2, 129.2, 129.1, 128.6, 128.4, 127.9, 127.6, 125.5, 125.2, 122.7, 114.8, 114.6, 111.8, 111.6, 110.2 ppm. HRMS (ESI^+): calcd. for $C_{39}H_{29}FN_6$, $[M+H]^+$ 601.2516, found 601.2506.

2-[*N,N*-(4-fluorophenyl)phenylamino)]-4,6-bis(diphenylamino)-1,3,5-trazine (HPM-*p*-F): 4-Fluoro-*N*-phenylaniline (374.4 mg, 2 mmol) and 10 mL dry THF were palced in a flame-dried Schlenk tube with a magnetic stir bar under a N_2 atmosphere. Then the solution was cooled to -20 °C and *n*-BuLi (2.5 M in hexane, 0.96 mL, 2.4 mmol) was dropped slowly into the solution. The mixture was then warmed to room temperature and 2-chloro-4,6-bis(diphenylamino)-1,3,5-trazine (899.9 mg, 2 mmol) was added. The mixture was heated at 60 °C overnight. A large amount of solid product was precipitated. The precipitation was

filtered and washed with methanol several times. The desired product was then recrystallized from xylene and dried in vacuo to give a white solid (722 mg, 60%). ^{1}H NMR (400 MHz, $CDCl_3$): δ = 7.10-7.16 (m, 20 H), 7.03-7.07 (m, 7H), 6.76-6.82 (m, 2H) ppm. ^{13}C NMR (100 MHz, $CDCl_3$): δ = 165.8, 165.7, 161.4, 158.9, 143.5, 143.3, 139.54, 139.51, 129.4, 129.3, 128.39, 128.36, 127.6, 127.3, 125.1, 125.0, 115.2, 115.0 ppm. HRMS (ESI$^+$): calcd. for $C_{39}H_{29}FN_6$, $[M+H]^+$ 601.2516, found 601.2512.

III. Photophysical Properties

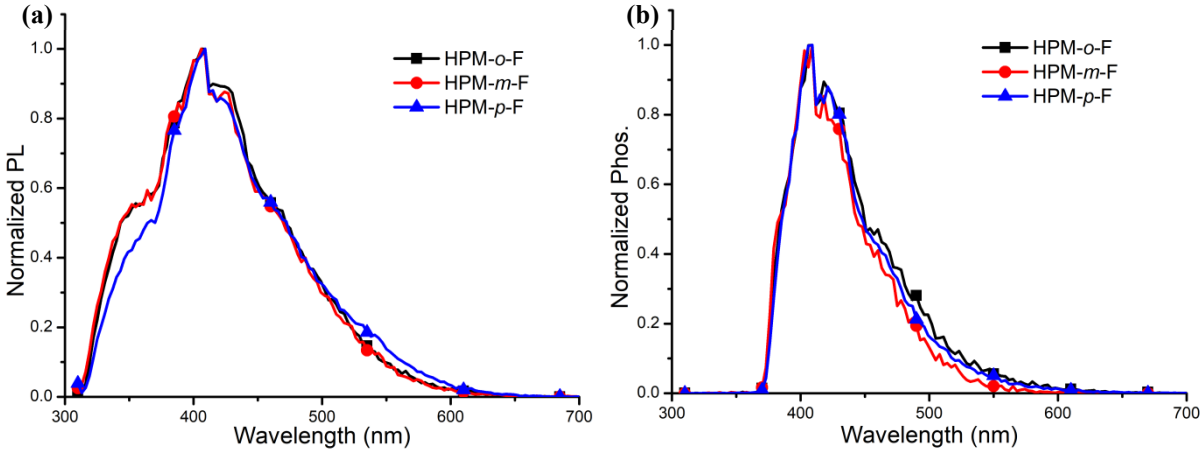

Fig. S1 The photoluminescence (PL) spectra of HPM-F isomers in diluted 2-MeTHF solution at 77 K with (a) a detector delay of 0 ms and (b) a detector delay of 20 ms.

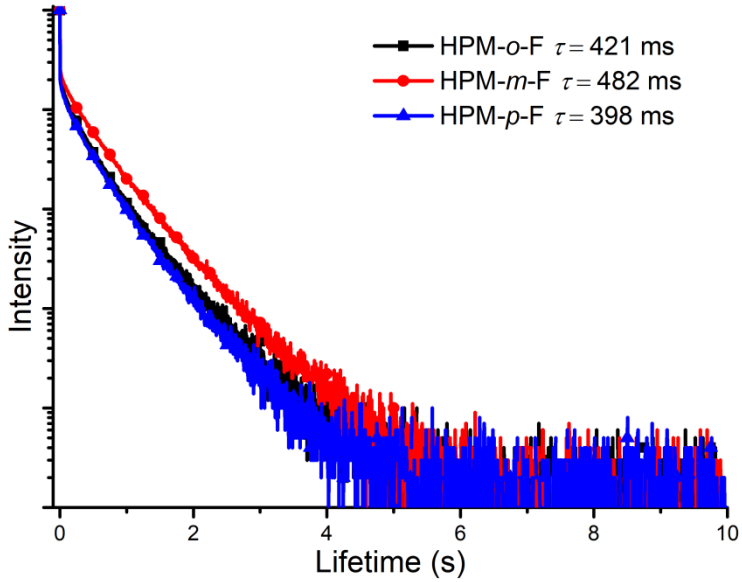

Fig. S2 The time-resolved PL decay curves of HPM-F isomers in diluted 2-MeTHF solution at 77 K at 407 nm.

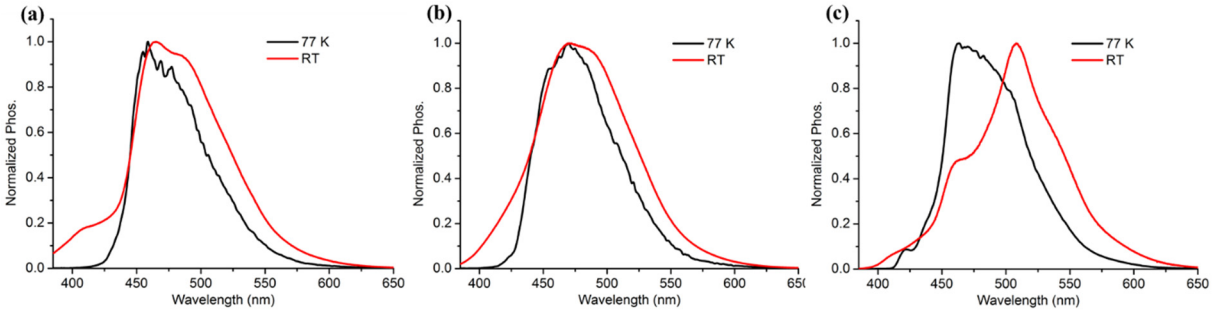

Fig. S3 The phosphorescence spectra of (a) HPM-*o*-F, (b) HPM-*m*-F and (c) HPM-*p*-F in crystal state at 77 K and room temperature (RT), respectively.

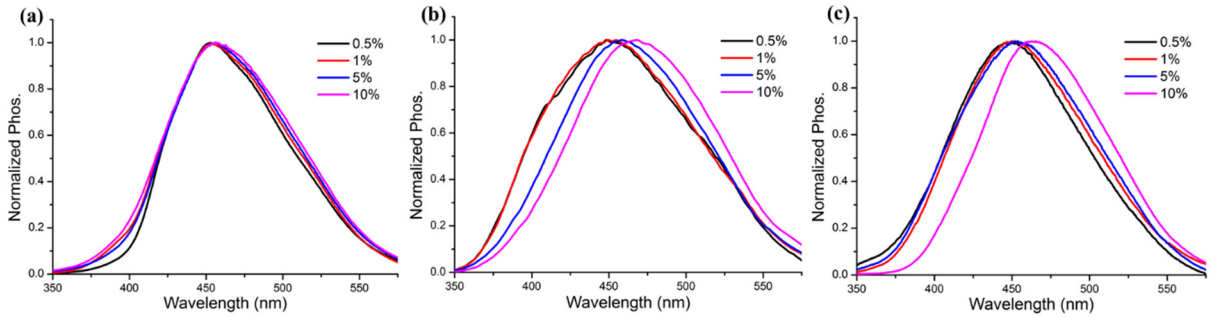

Fig. S4 The phosphorescence spectra of (a) HPM-*o*-F, (b) HPM-*m*-F and (c) HPM-*p*-F at different doping concentrations (mass percent) in PMMA films.

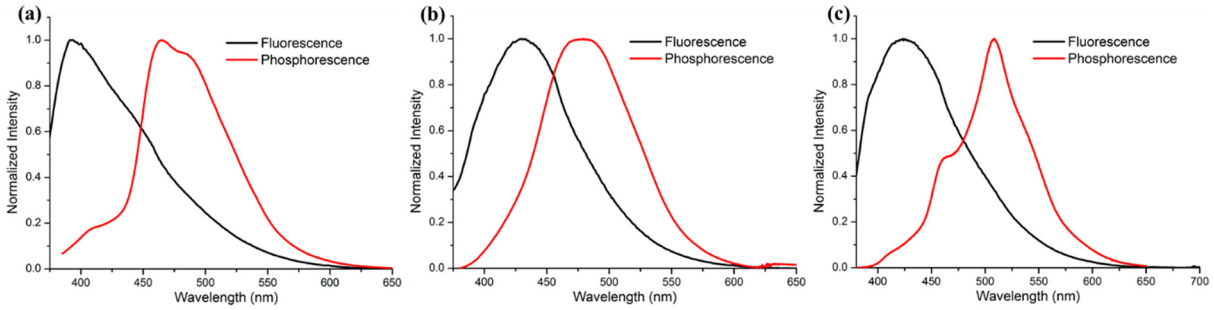

Fig. S5 The fluorescence and phosphorescence spectra of (a) HPM-*o*-F, (b) HPM-*m*-F and (c) HPM-*p*-F in crystal state under ambient conditions. The estimated energy gaps between the singlet and triplet states (ΔE_{ST}), determined from the fluorescence and phosphorescence peak energies, were 0.50, 0.29, and 0.28 eV for HPM-*o*-F, HPM-*m*-F, and HPM-*p*-F, respectively.

Table S1 The details of RTP lifetimes of HPM-F isomers in 2-MeTHF solution and crystals.

State	Compound	λ_{phos} (nm)	τ_1 (ms)	A_1	τ_2 (ms)	A_2	τ^a (ms)
Solution[b]	HPM-*o*-F	407	220.1	0.39	550.0	0.61	421
	HPM-*m*-F	407	259.7	0.33	591.4	0.67	482
	HPM-*p*-F	407	197.6	0.33	498.8	0.67	398
Crystal[c]	HPM-*o*-F	465	39.2	0.67	185.8	0.33	88
	HPM-*m*-F	479	14.0	0.73	177.1	0.27	58
	HPM-*p*-F	468	45.7	0.79	311.5	0.21	103
		507	80.7	0.63	456.4	0.37	220

[a] The average lifetime $\tau = \tau_1 \times A_1 + \tau_2 \times A_2$; [b] at 77 K; [c] under ambient condition.

Table S2 Single crystal data of HPM-F isomers.

Name	HPM-*o*-F	HPM-*m*-F	HPM-*p*-F
Formula	$C_{39}H_{29}FN_6$	$C_{39}H_{29}FN_6$	$C_{39}H_{29}FN_6$
Space Group	*R*-3*c*	*R*-3*c*	*R*-3*c*
Cell Lengths (Å)	a=14.3978(4) b=14.3978(4) c= 25.6230(11)	a=14.3814(4) b=14.3814(4) c=25.5525(13)	a=14.5389(9) b=14.5389(9) c=25.5523(16)
Cell Angles (°)	a =90 b =90 c =120	a =90 b =90 c =120	a =90 b =90 c =120
Cell Volume (Å^3)	4599.9(3)	4576.8(3)	4677.6(6)
Z	6	6	6
Density (g/cm^3)	1.301	1.308	1.279
F(000)	1884.0	1884.0	1884.0
h_{max}, k_{max}, l_{max}	18,18,33	18,18,33	17,17,31
CCDC number	2392815	2392813	2063809
Refinement details:	1. Fixed Uiso At 1.2 times of: All C(H) groups, All F(H) groups 2. Restrained distances C3-H3 0.94 with sigma of 0.001 3. Others Fixed Sof: F1(0.16667) H3(0.83333) 4.a Aromatic/amide H refined with riding coordinates: C7(H7), C6(H6), C4(H4), C5(H5)	1. Fixed Uiso At 1.2 times of: All C(H) groups, All F(H) groups 2. Restrained distances C6-H6 0.94 with sigma of 0.001 3. Others Fixed Sof: F1(0.16667) H6(0.83333) 4.a Aromatic/amide H refined with riding coordinates: C3(H3), C4(H4), C5(H5), C7(H7)	1. Fixed Uiso At 1.2 times of: All C(H) groups 2. Restrained distances C5-F1 1.38 with sigma of 0.02 3. Others Fixed Sof: H5(0.83333) F1(0.16667) 4. a Aromatic/amide H refined with riding coordinates: C3(H3), C4(H4), C5(H5), C6(H6), C7(H7)

IV. Theoretical calculations

The molecular coordinates of HPM-F isomers used for theoretical calculations were obtained from single-crystal data, with the coordinates of carbon and nitrogen atoms kept fixed while the positions of hydrogen and fluorine atoms were optimized using the PM7 semi-empirical method with the Gaussian 16 A.03 package [S8]. To optimize the S_0, S_1 and T_1 geometries of the structures in solid states, a QM/MM method using a two-layer ONIOM approach based on the single-crystal data was employed. The central molecule was treated as the high layer and calculated using the QM method at the B3LYP-D3(BJ)/6-31G* level for the S_0 state and TDDFT B3LYP-D3(BJ)/6-31G* level for the S_1 and T_1 state, repectively. Meanwhile, the surrounding molecules were frozen, treated as the low layer, and calculated using the MM method (UFF, embedded QEq charge) with the Gaussian package. The independent gradient model based on Hirshfeld partition (IGMH), natural transition orbitals (NTO) of HPM-F dimers were obtained by Multiwfn program and VMD program [S9-11]. The basis set superposition error (BSSE) corrected binding energies of dimers($\Delta E_{bind,dimer}$) of HPM-F isomers were calculated to estimate the strength of noncovalent intermolecular interactions with functional and basis set of M06-2X(BJ)/6-311+G(d,p). The excitation energies for the singlet and triplet states were calculated using the TDDFT B3LYP-D3(BJ)/6-31G* method based on the optimized molecular structure at the S_0 and T_1 state, respectively, with the Gaussian package. The oscillator strength of the triplet states (T_1) were calculated at the TDDFT B3LYP/cc-pVDZ level based on the optimized T_1 molecular structure using Dalton program [S12]. The spin-orbit coupling (SOC) matrix elements between S_1 and T_n, as well as T_1 and S_0, were calculated at the TDDFT B3LYP/6-311G** level, based on the optimized S_1 and T_1 molecular structures, respectively, using the Dalton program.

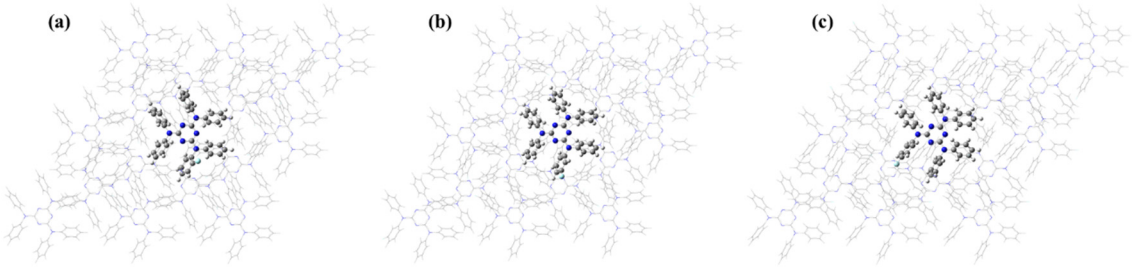

Fig. S6 QM/MM model for crystal (a) HPM-*o*-F, (b) HPM-*m*-F, (c) HPM-*p*-F, respectively.

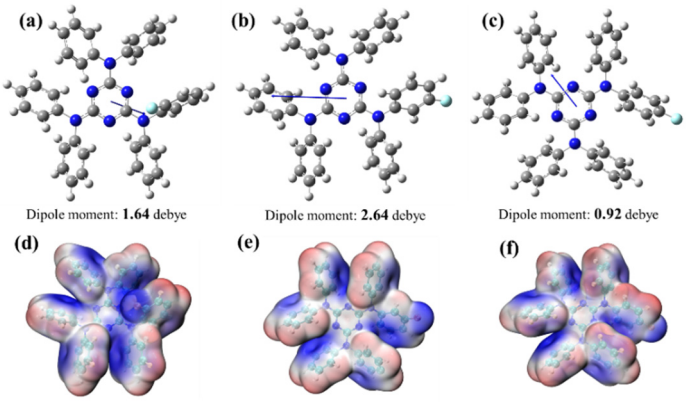

Fig. S7 Calculated dipole moment of (a) HPM-o-F, (b) HPM-m-F, (c) HPM-p-F and electroostatic potential (ESP) diagram of (d) HPM-*o*-F, (e) HPM-*m*-F, (f) HPM-*p*-F at gas phase. (The potential energy range is -0.03 to 0.03 a.u. . Red areas indicate high electron density and blue areas suggest low electron density).

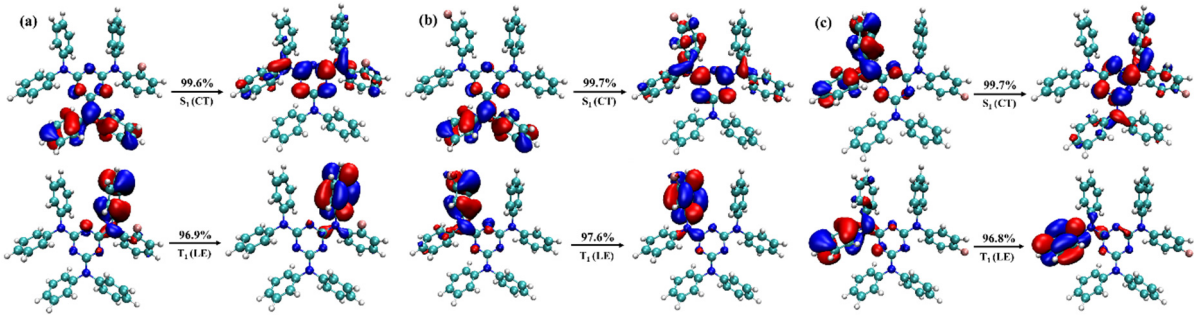

Fig. S8 Calculated natural transition orbitals (NTO) of the S_1 (based on S_1 geometry) and T_1 (based on T_1 geometry) of (a) HPM-*o*-F, (b) HPM-*m*-F, (c) HPM-*p*-F, respectively, monomer at QM(B3LYP/6-31G*)/MM level.

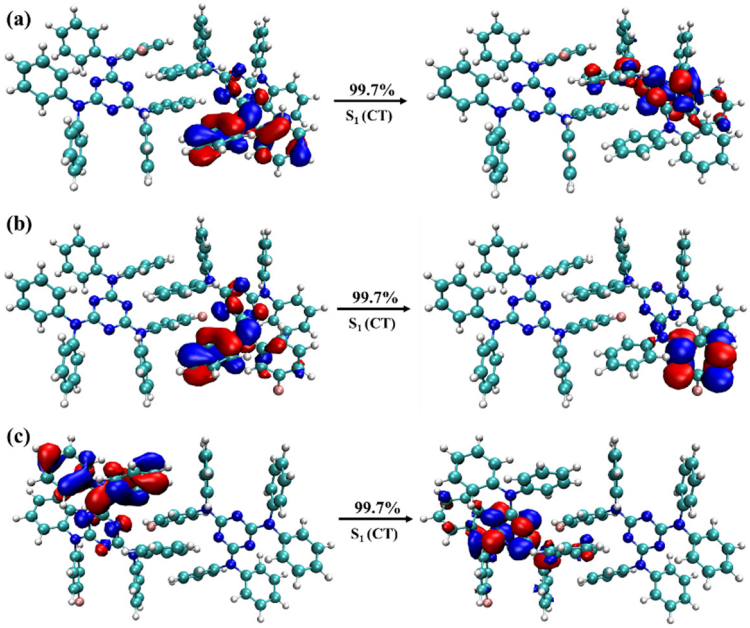

Fig. S9 Calculated NTOs of the S_1 (based on S_1 geometry) of (a) HPM-*o*-F, (b) HPM-*m*-F, (c) HPM-*p*-F, respectively, dimer at QM(B3LYP/6-31G*)/MM level.

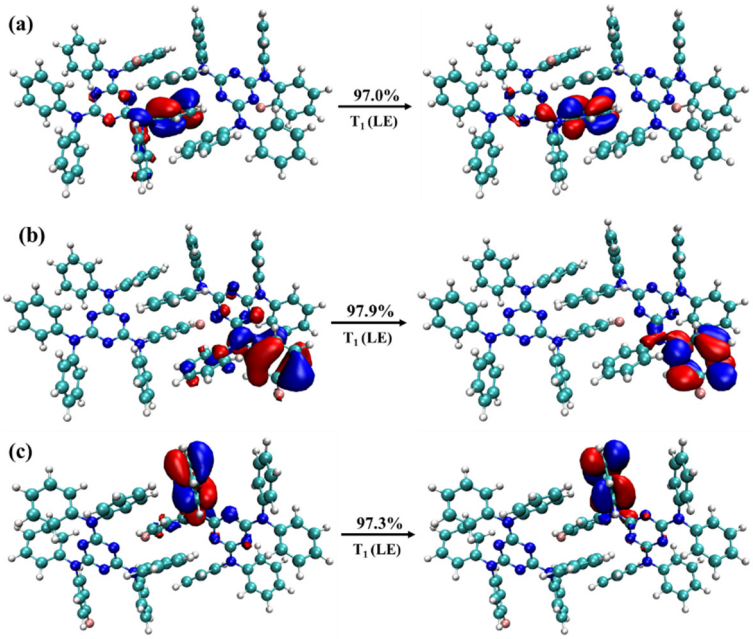

Fig. S10 Calculated NTOs of the T_1 (based on T_1 geometry) of (a) HPM-*o*-F, (b) HPM-*m*-F, (c) HPM-*p*-F, respectively, dimer at QM(B3LYP/6-31G*)/MM level.

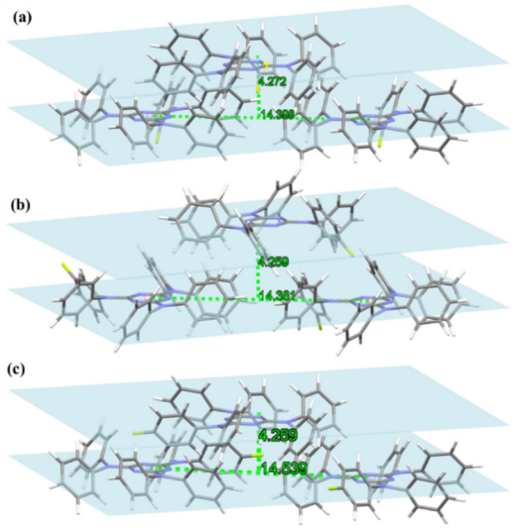

Fig. S11 The local packing pictures were selected from the parts in cycles of corresponding entire ones, in which the interlamellar spacing and centroid–centroid distances of the involved triazine rings are listed (unit: Å). (a) HPM-*o*-F, (b) HPM-*m*-F, (c) HPM-*p*-F.

Table S3 Intermolecular interactions and Hirshfeld surface analysis of HPM-*o*-F and HPM-*m*-F at crystalline state.

	HPM-*o*-F	HPM-*m*-F
Intermolecular interactions	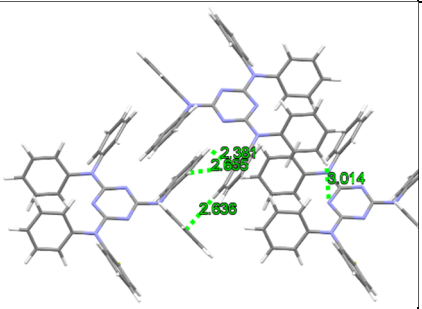	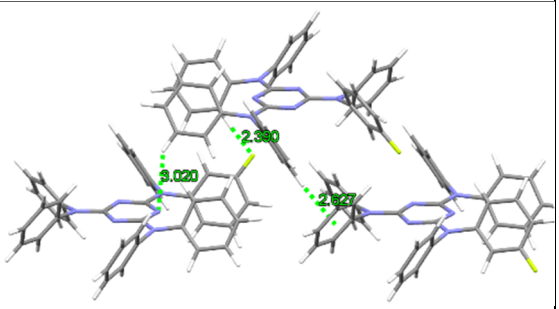
Hirshfeld surface	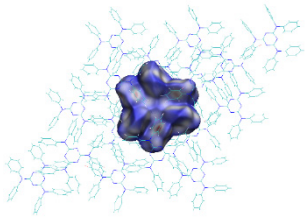	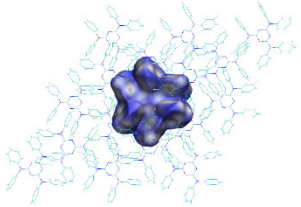
Fingerprint plot	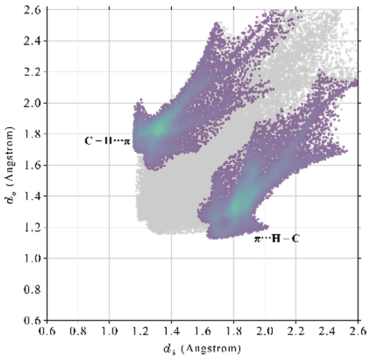	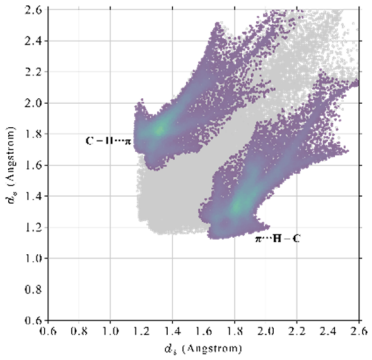
Fingerprint plot	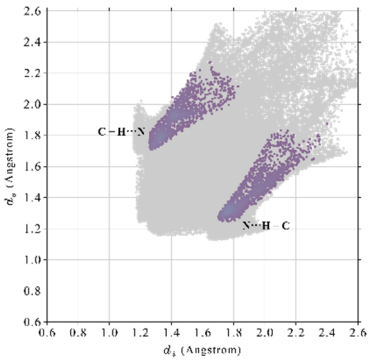	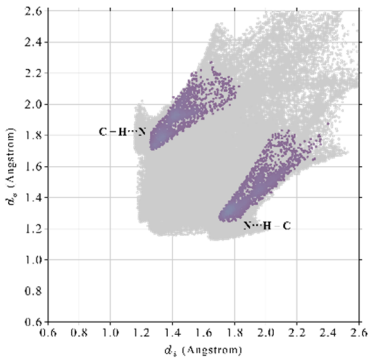
Relative contributions to the Hirshfeld surface area for the various close intermolecular contacts	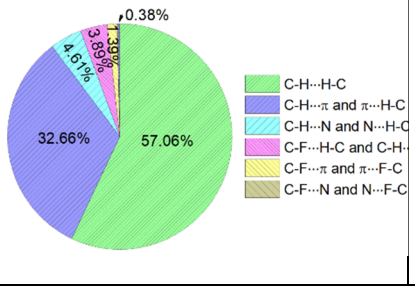	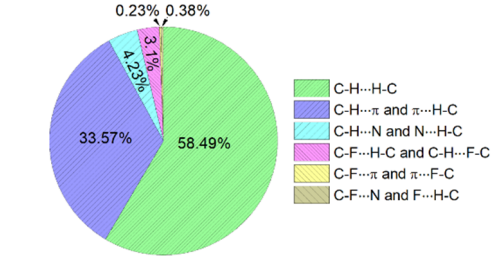

Table S4 The IGMH and BSSE corrected binding energies of dimers ($\Delta E_{bind,dimer}$) of HPM-F isomers in the adjacent layers or same layer.

	HPM-*o*-F	HPM-*m*-F	HPM-*p*-F
Adjacent layers	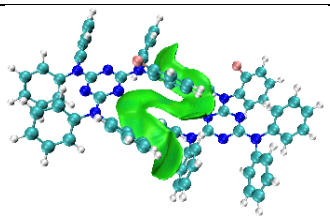 $\Delta E_{bind,dimer}$ = -15.74 kcal / mol	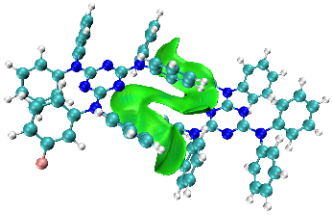 $\Delta E_{bind,dimer}$ = -15.51 kcal / mol	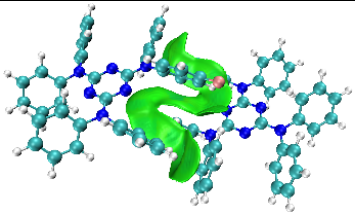 $\Delta E_{bind,dimer}$ = -16.46 kcal / mol
Same layer	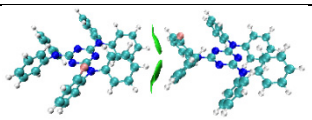 $\Delta E^{parallel}_{bind,dimer}$ = - 2.64 kcal / mol	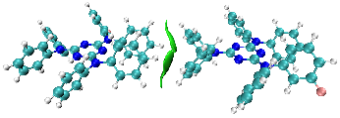 $\Delta E^{parallel}_{bind,dimer}$ = - 2.74 kcal / mol	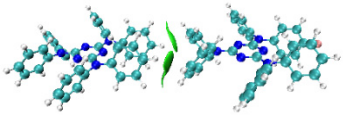 $\Delta E^{parallel}_{bind,dimer}$ = - 2.53 kcal/mol

V. References

[S1] X. Kong, H. Zhang, Y. Xiao, C. Cao, Y. Shi, G. Pang, *RSC Adv.*, 2015, **5**,7035–7048.

[S2] J. Cao, J. R. Lever, T. Kopajtic, J. L. Katz, A. T. Pham, M. L. Holmes, J. B. Justice, A. H. Newman, *J. Med. Chem.,* 2004, **47**, 6128–6136.

[S3] Z-F. An, R.-F Chen, J. Yin, G.-H. Xie, H.-F. Shi, T. Tsuboi, W. Huang, *Chem. Eur. J.,* 2011, **17**, 10871–10878.

[S4] O. V Dolomanov, L. J. Bourhis, R. J. Gildea, J. A. K. Howard, H. Puschmann, *J. Appl. Cryst.,* 2009, **42**, 339–341.

[S5] G. M. Sheldrick, *Acta Cryst. A,* 2015, **71**, 3–8.

[S6] G. M. Sheldrick, *Acta Cryst. C*, 2015, **71**, 3–8.

[S7] L. J. Bourhis, O. V. Dolomanov, R. J. Gildea, J. A. K. Howard, H. Puschmann, *Acta Cryst. A*, 2015, **71**, 59-75.

[S8] Gaussian 16, Revision A.03, M. J. Frisch, G. W. Trucks, H. B. Schlegel, G. E. Scuseria, M. A. Robb, J. R. Cheeseman, G. Scalmani, V. Barone, G. A. Petersson, H. Nakatsuji, X. Li, M. Caricato, A. V. Marenich, J. Bloino, B. G. Janesko, R. Gomperts, B. Mennucci, H. P. Hratchian, J. V. Ortiz, A. F. Izmaylov, J. L. Sonnenberg, D. Williams-Young, F. Ding, F. Lipparini, F. Egidi, J. Goings, B. Peng, A. Petrone, T. Henderson, D. Ranasinghe, V. G. Zakrzewski, J. Gao, N. Rega, G. Zheng, W. Liang, M. Hada, M. Ehara, K. Toyota, R. Fukuda, J. Hasegawa, M. Ishida, T. Nakajima, Y. Honda, O. Kitao, H. Nakai, T. Vreven, K. Throssell, J. A. Montgomery, Jr., J. E. Peralta, F. Ogliaro, M. J. Bearpark, J. J. Heyd, E. N. Brothers, K. N. Kudin, V. N. Staroverov, T. A. Keith, R. Kobayashi, J. Normand, K. Raghavachari, A. P. Rendell, J. C. Burant, S. S. Iyengar, J. Tomasi, M. Cossi, J. M. Millam,

M. Klene, C. Adamo, R. Cammi, J. W. Ochterski, R. L. Martin, K. Morokuma, O. Farkas, J. B. Foresman, and D. J. Fox, Gaussian, Inc., Wallingford CT, 2016.

[S9] T. Lu, Q. Chen, *J. Comput. Chem.*, 2022, **43**, 539-555

[S10] T. Lu, F. Chen, *J. Comput. Chem.* 2012, **33**, 580-592. Multiwfn 3.8 (dev) program: http://sobereva.com/multiwfn/ .

[S11] VMD 1.9.3 program: http://www.ks.uiuc.edu/Research/vmd/ .

[S12] K. Aidas, C. Angeli, K. L. Bak, V. Bakken, R. Bast, L. Boman, O. Christiansen, R. Cimiraglia, S. Coriani, P. Dahle, E. K. Dalskov, U. Ekstroem, T. Enevoldsen, J. J. Eriksen, P. Ettenhuber, B. Fernandez, L. Ferrighi, H. Fliegl, L. Frediani, K. Hald, A. Halkier, C. Haettig, H. Heiberg, T. Helgaker, A. C. Hennum, H. Hettema, E. Hjertenaes, S. Hoest, I.-M. Hoeyvik, M. F. Iozzi, B. Jansik, H. J. Aa. Jensen, D. Jonsson, P. Joergensen, J. Kauczor, S. Kirpekar, T. Kjaergaard, W. Klopper, S. Knecht, R. Kobayashi, H. Koch, J. Kongsted, A. Krapp, K. Kristensen, A. Ligabue, O. B. Lutnaes, J. I. Melo, K. V. Mikkelsen, R. H. Myhre, C. Neiss, C. B. Nielsen, P. Norman, J. Olsen, J. M. H. Olsen, A. Osted, M. J. Packer, F. Pawlowski, T. B. Pedersen, P. F. Provasi, S. Reine, Z. Rinkevicius, T. A. Ruden, K. Ruud, V. Rybkin, P. Salek, C. C. M. Samson, A. Sanchez de Meras, T. Saue, S. P. A. Sauer, B. Schimmelpfennig, K. Sneskov, A. H. Steindal, K. O. Sylvester-Hvid, P. R. Taylor, A. M. Teale, E. I. Tellgren, D. P. Tew, A. J. Thorvaldsen, L. Thoegersen, O. Vahtras, M. A. Watson, D. J. D. Wilson, M. Ziolkowski, H. Agren, "The Dalton quantum chemistry program system", *WIREs Comput. Mol. Sci.* 2014, **4**, 269–284; and Dalton, a molecular electronic structure program, Release Dalton2019.alpha (2019), see http://daltonprogram.org.

VI. Copies of ^{1}H, ^{13}C NMR and HRMS spectra of HPM-F isomers.

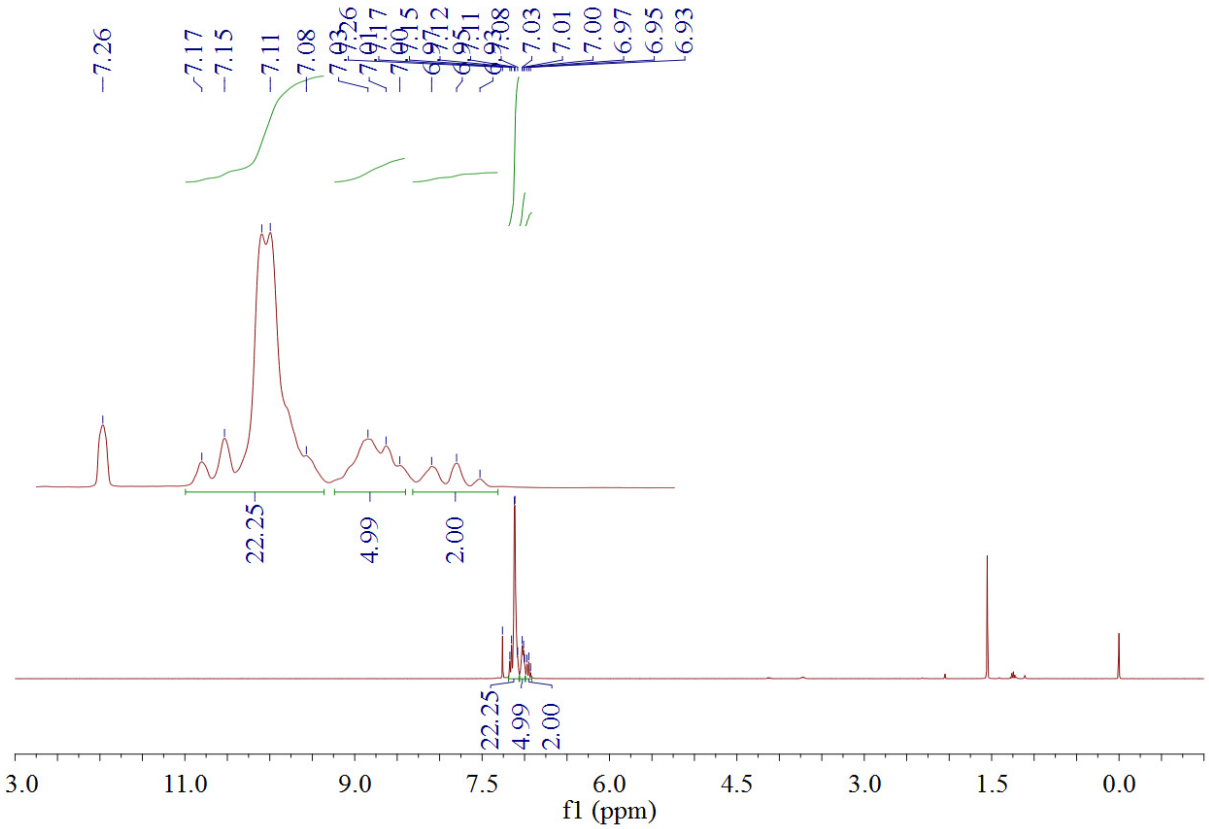

Fig. S12 ^{1}H NMR spectrum of HPM-*o*-F in $CDCl_3$.

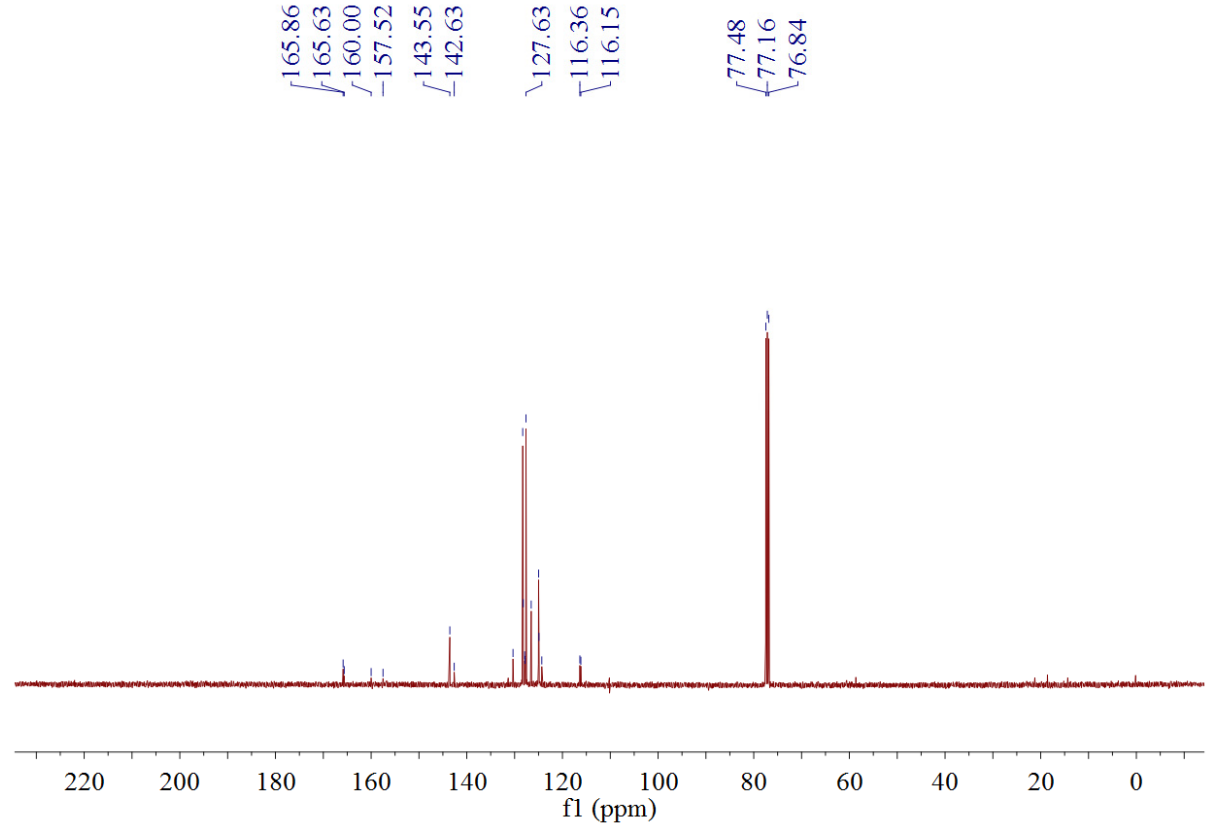

Fig. S13 ^{13}C NMR spectrum of HPM-*o*-F in $CDCl_3$.

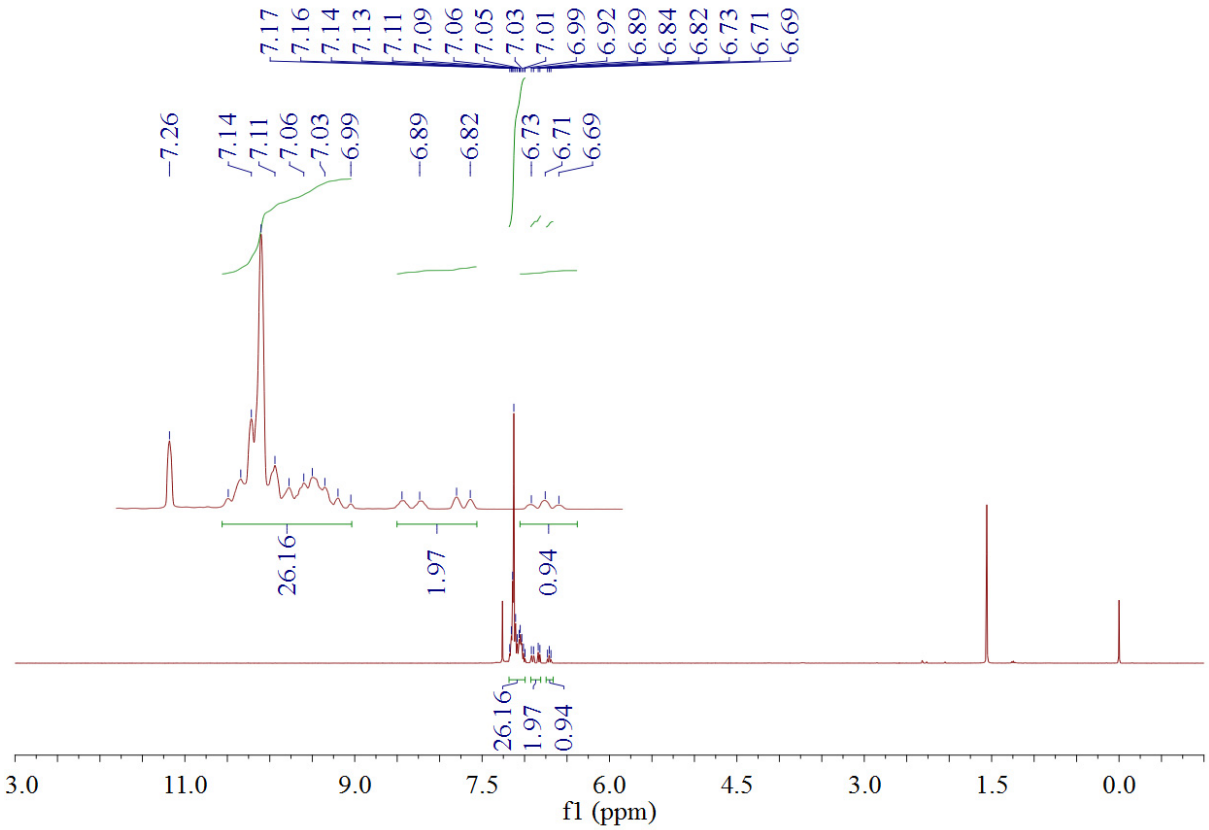

Fig. S14 ^{1}H NMR spectrum of HPM-*m*-F in $CDCl_3$.

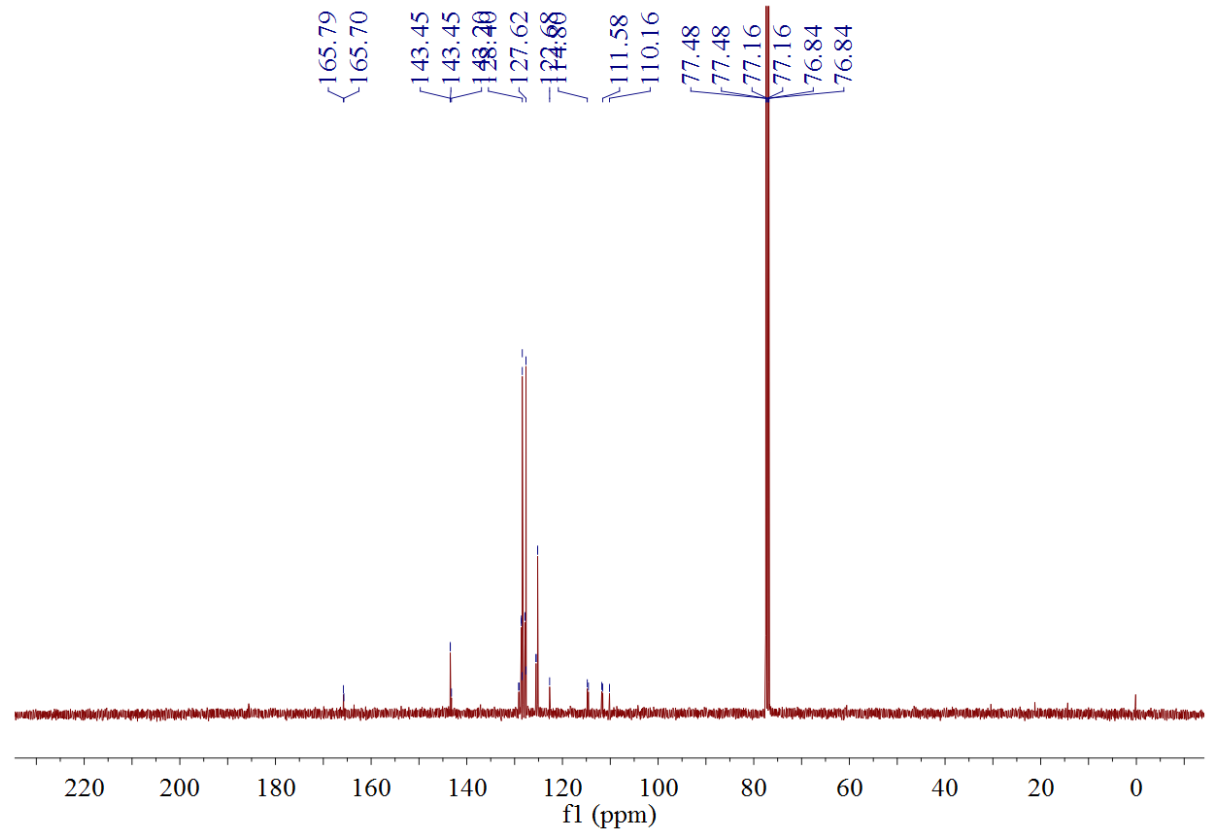

Fig. S15 ^{13}C NMR spectrum of HPM-*m*-F in $CDCl_3$.

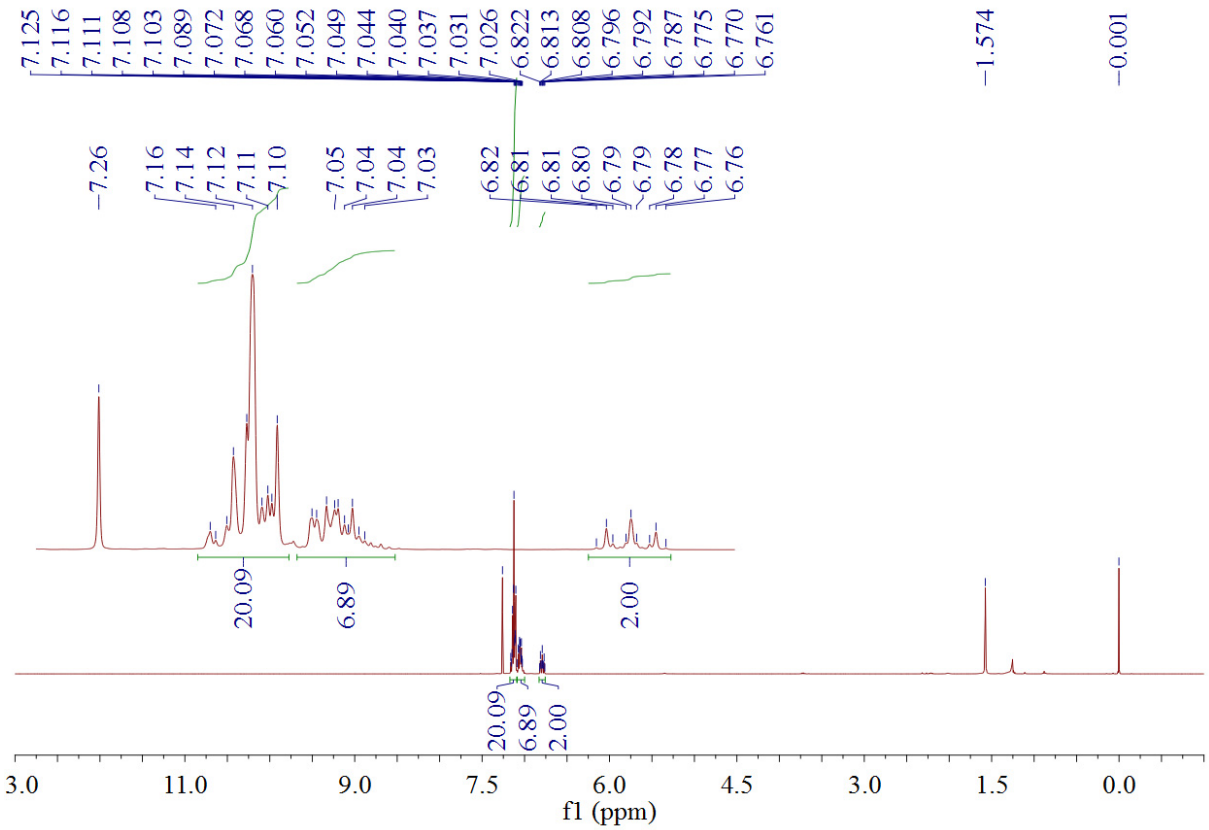

Fig. S16 ^{1}H NMR spectrum of HPM-*p*-F in $CDCl_3$.

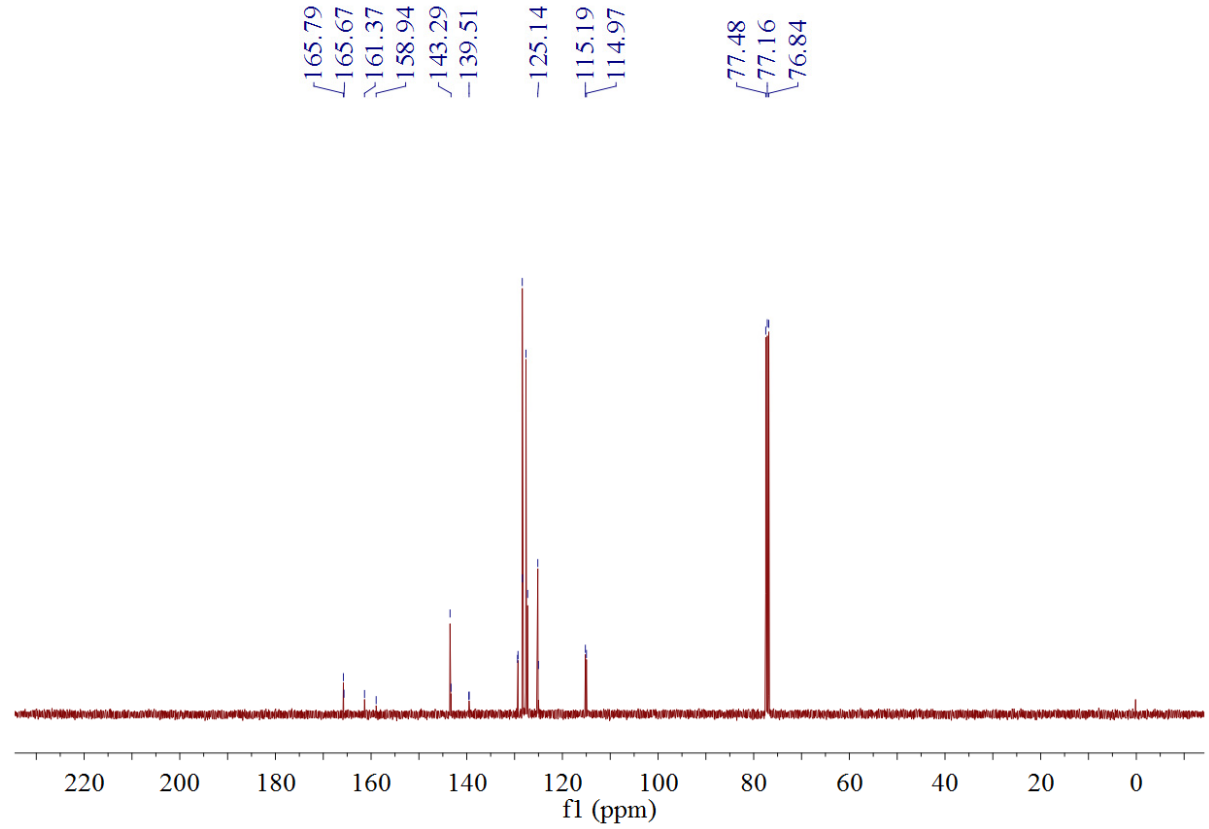

Fig. S17 ^{13}C NMR spectrum of HPM-*p*-F in $CDCl_3$.

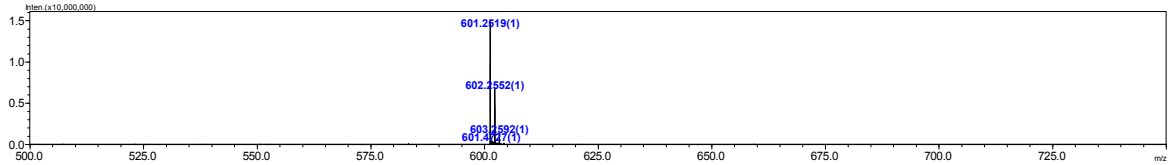

Fig. S18 High-resolution mass spectrum of HPM-*o*-F

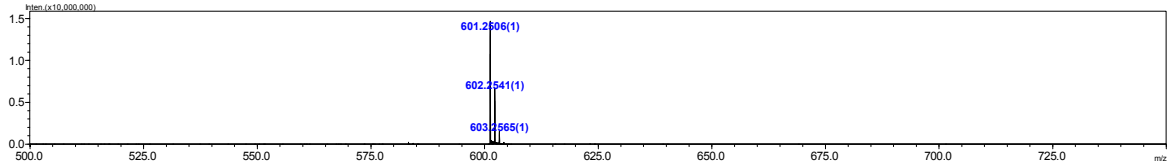

Fig. S19 High-resolution mass spectrum of HPM-*m*-F

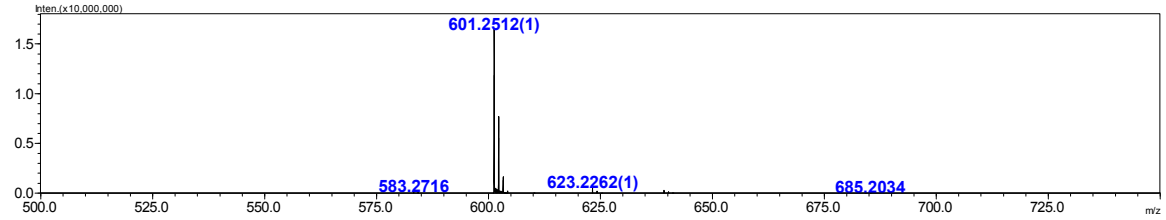

Fig. S20 High-resolution mass spectrum of HPM-*p*-F